Postprint of: Sadeghi B., Cavaliere P., Laska A., Perrone A., Blasi G., Gopinathan A., Shamanian M., Ashrafizadeh F., Effect of processing parameters on the cyclic behaviour of aluminium friction stir welded to spark plasma sintered aluminium matrix composites with bimodal micro-and nano-sized reinforcing alumina particles, MATERIALS CHARACTERIZATION, Vol. 195 (2023), 112535, DOI: 10.1016/j.matchar.2022.112535

Effect of processing parameters on the cyclic behaviour of aluminium friction stir welded to spark plasma sintered aluminium matrix composites with bimodal micro-and nano-sized reinforcing alumina particles

B. Sadeghi [a,*], P. Cavaliere [b,*], A. Laska [c], A. Perrone [b], G. Blasi [b], A. Gopinathan [d], M. Shamanian [e], F. Ashrafizadeh [e]

a Centre of Excellence for Advanced Materials Application, Slovak Academy of Sciences, Dubravska Cesta 9, 84511 Bratislava, Slovak Republic

b Department of Innovation Engineering, University of Salento, Via per Arnesano, 73100 Lecce, Italy

c Faculty of Mechanical Engineering and Ship Technology, Gdansk University of Technology, Narutowicza 11/12, 80-233 Gda´nsk, Poland

d Institute of Materials and Machine Mechanics, The Slovak Academy of Sciences, Dubravska cesta 9, 84513 Bratislava, Slovak Republic

e Department of Material Engineering, Isfahan University of Technology, Isfahan, Iran

Abstract:

Understanding the cyclic behaviour of Alumina reinforced Aluminium composites (Al-A2O3) was of critical importance, for their further application in the different industrial sectors. The present study is focussing on the cyclic behaviour of the Al-Alumina nanocomposite produced through the combination of spark plasma sintering (SPS) method and friction stir welding (FSW). The added Alumina with total content of 10% is the combination of nano and micro-sized particles and its ratio differ for each sample. The microstructure of the SPSed samples is characterized using optical microscopy (OM), scanning electron microscopy (SEM), and energy dispersive X-ray spectroscopy (EDS). The microstructure of the processed composite samples is characterized and its mechanical behaviour is studied. Microstructural studies showed that nano sized particles of Alumina were mostly distributed along the grain boundaries and inside the grains, while micron-sized ones mostly settled on the grain boundaries. In addition, the hardness and tensile properties of the produced samples are analysed concerning the reinforcement size and the percentage of nanoparticles addition. The obtained results reveal that the mechanical and fatigue properties of the nanocomposite materials mainly depend on the material properties at the initial stage and the applied conditions of friction stir welding such as rotating speed and movement speed. The facture surface of the nanocomposites revealed a combined ductile–brittle fracture mode with finer dimples with emphasis on the pronounced role of nano-metric dispersoids.

Keywords: Spark plasma sintering, Friction stir welding, Nanocomposites, Microstructure, Fatigue

1. Introduction

The developed MMCs need to be joined for various industrial applications of various automobile and aerospace industries due to its low density, high strength, specific modulus, etc. [1,2]. Since fatigue induced failure of engineering structures reaches ~90% [1], therefore, it is vital to investigate the fatigue properties of friction stir welded (FSWed) metal matrix composites (MMCs) joints for the safe

and reliable structural applications. Spark plasma sintering (SPS) is a powder metallurgy technique allowing for the production of metal matrix composites [3]. SPS uses a lower temperature to achieve nanostructured materials with better mechanical properties in a short sintering time. It is a non-conventional technique that achieves high temperature in lesser time by combining the heating rates (100 ◦C/min) with the external pressure [4,5]. Through the precise control of process parameters, it is possible to strongly reduce the material porosity and induce nano-structuring of grains [6–8]. In recent days, the usage of MMCs is increased in various sectors such as the automotive and aerospace industries. Lightweight MMCs possess very good mechanical properties [9]. The deteriorated fatigue performance that is one of critical bottleneck restricting the prospective applications of ultrafine (UFG) MMCs can be originated from microstructural defects such as agglomeration of dispersoids, porosity, etc. [10,11]. The presence of porosity is the,deciding factor in the MMC's mechanical and cyclic performance [10,12]. In our recent paper [13], the effect of porosity on the thermomechanical behaviour of friction stir welded spark plasma sintered aluminium matrix composites with bimodal micro-and nano-sized reinforcing Al2O3 particles was studied, and the results experimentally and simulation demonstrated that by increasing the tool rotating speed and the welding speed heat input and thermo-mechanical stresses increase in the material which in turn improve material mixing (both matrix and reinforcement) and reduce the porosity content. In turn, it causes a defect-free, fine-grained, uniform distribution of nanosized and microsized Al2O3 particles, and higher hardened weld nugget region. Thus, the porosity needs to be effectively controlled to get the desirable properties of the MMCs.

As per the knowledge of the authors, most of researches performed on effect of processing parameters are focused on the evolution of microstructure and mechanical properties of SPSed Al based composites [3,14,15]. Less information is available in literature concerning the cyclic behaviour of MMCs produced by powder metallurgy technique [10,16]. Despite some research works studied the effect of processing parameters during FSW of Al based materials [3,17–21], there was no work concerned about the effect of processing parameters on the cyclic behaviour of bimodal sized Al2O3/Al nanocomposites fabricated through the combination of SPS and FSW. Moreover, because of thestructural components experience dynamic loading, which results in the occurrence of fatigue failure, an understanding of fatigue and cyclic deformation behaviour of AMMCs is critical for the design, durability evaluation and life prediction of engineering components [16,22]. The fatigue behaviour of the powder metallurgy Al based composites needs to be studied for their structural applications, and further application in the different industrial sectors.

Various strengthening mechanisms in aluminium based MMCs are mentioned, and some of them are Orowan strengthening, grain boundary strengthening and hardening [23,24]. Strengthening in SPSed composites is achieved through grain refinement and the Orowan mechanism depending on the dimensions of the reinforcing phase [25,26]. It is largely demonstrated that a further increase in mechanical properties can be achieved through friction stir welding (FSW) [26–28]. This is amplified by the employment of nanosized reinforcements to the metallic matrix [28–30]. So, the pronounced grain refinement and the optimal reinforcing phases distribution through FSW lead to an increase in the material's mechanical properties [31,32]. Composites with either nano-sized or micro-sized particles alone resulted in agglomeration which act as stress concentration sources which eventually reduce the strength of compacted samples [16,33–35]. In this view, the contemporary addition of micro-sized and nanosized reinforcing powders is demonstrated to be more effective at the same volume percentage [36]. So, here it is clear how the final properties of the fabricated nanocomposites depend on the percentage of the nano to micron reinforcement and also on the process parameters such as rotating and travelling speeds as well as processing forces. In addition, the optimal distribution of nanosized reinforcements leads to the improvement in fatigue life [37]. It has been highlighted that the fatigue

life increase is due to the coupled effect of nanoparticles distribution and their effect on grain refinement [38]. Therefore, in the current paper, the combination of nano and micron-sized reinforcing proposed to study the effect of combination of two size reinforcing on cyclic behaviour and microstructural development. Here, a pronounced strengthening effect is achieved also through the minor addition of nanoparticles [33,39].

The ease and scalability of the powder metallurgy technique is one of the most popular methods of manufacturing MMCs, which can be used by controlling process parameters [14,15], microstructure engineering [24,40,41] and reinforcements [42,43] can be used as a reliable and industrial technique in order to produce strong materials with high fatigue resistance. From the scientific point of view, the weak cyclic behaviour such as cyclic softening originated from the microstructure instability in terms of grain coarsening and shear banding that are the inherent fatigue damage mechanisms of the UFG materials [12,44] especially MMCs [45,46]. To the best authors' knowledge, less scientific evidence on the fatigue behaviour of bimodal (micro and nano-sized) reinforced aluminium alloys produced via powder metallurgy and frictionstir welding are presented in the literature. Therefore, in advanced application of MMCs, assessing the fatigue properties remains a challenge, as both strength and ductility are important. Our early investigation indicated that the FSWed Al matrix composites produced via SPS presented limited porosity, which in turn develops a defect-free, finegrained, uniform distribution of nano-sized and micro-sized Al2O3 particles, and a more hardened weld nugget region [13].

Motivated by the dependency of cyclic behaviour to microstructure which in turn depends on the processing parameters, the main objective of the current study is aimed to studying a cyclic behaviour of bimodal sized Al2O3/Al nanocomposites fabricated through the combination of SPS and FSW. Precisely, the present paper aims to describe the fatigue behaviour of aluminium reinforced with 6% of nanoparticles and 4% of microparticles of Alumina produced SPS and FSW. The microstructural features of the nanocomposites were characterized and their mechanical strengths under tensile loading were measured. Then, fatigue loading was carried out at a stress-controlled and strain-controlled modes with a stress ratio of R = 0.1 via a 3-point bending fatigue test.

2. Experimental procedure

Pure aluminium-Alumina composites were produced by employing pre aluminium particles produced via air atomization (ECKA, Germany) with the addition of 6% in volume of Alumina nanoparticles with mean dimensions of 20 nm (Evonik Industries, Germany) and 4% in volume of Alumina microparticles with mean dimensions of 10 mm (Feurth, Germany) through spark plasma sintering (SPS). The employed SPS procedure is detailed in previously published papers [26,47,48]. Cylindrical samples with 40 mm in diameter and 5 mm in thickness were produced. Then they were friction stir welded (FSWed) to pure aluminium sheets with the same thickness as shown in Fig. 1.

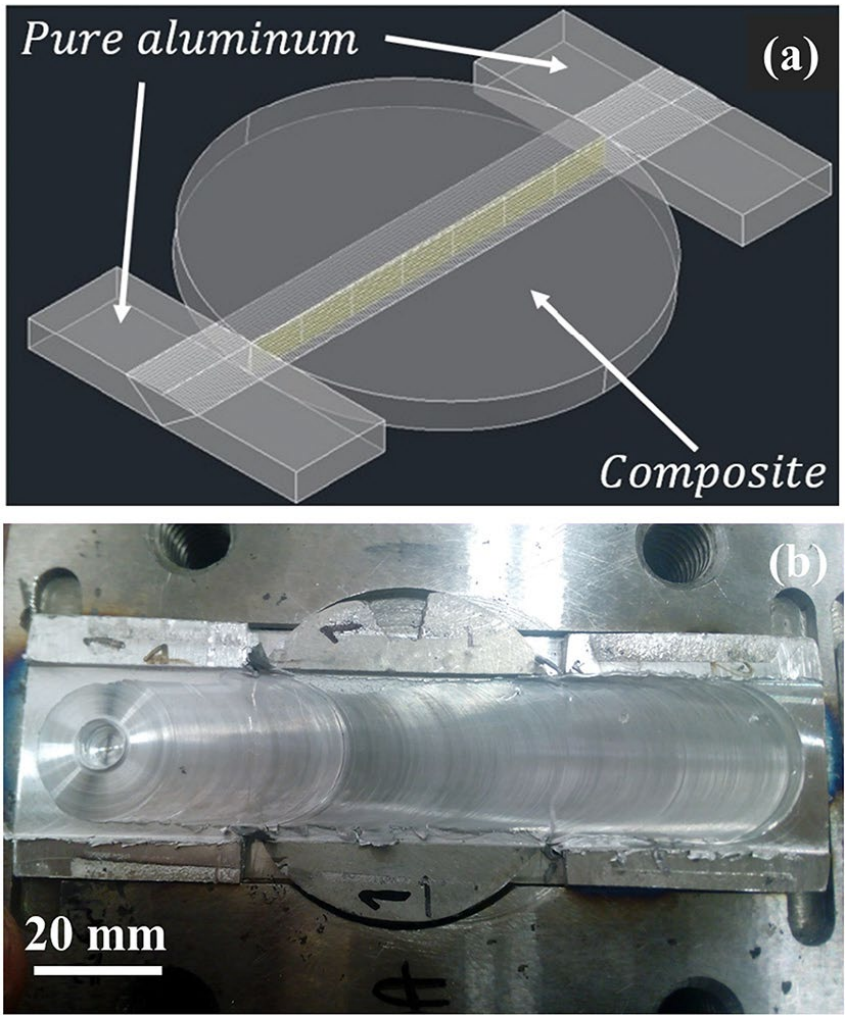

Fig. 1. FSW schematic and specimen preparation a); aspect of the weld after FSW b).

As shown in Fig. 1b, the regions far from the weld sections are friction stir processes from both sides of the pure aluminium and at the centre of the composite disk.

The employed tool geometry was described in [27,48], it had a conical-shaped tool. The employed tilt angle was 3◦. The welds were produced on a milling machine (Ferrari, Italy). The employed welding/ processing parameters are listed in Table 1.

Table 1
Revolutionary pitch as a funtion of the rotating and travel speed

Rotating speed (RPM)	Travel speed (mm/min)	Revolutionary pitch
2000	40	50
1900	50	38
1900	37	51.35
1600	32	50
1500	37	40.54
1500	32	46.87

These processing parameters were chosen because of previous results regarding the soundness of the welds [27]. The material's microstructure was characterized through optical and scanning electron microscopy (SEM, Zeiss EVO 40). In addition, the fracture surfaces of the tested materials were

observed through SEM. For transmission electron microscopy (TEM, JEOL JEM-2200FS, 200 kV) thin slice of thickness 0.125 mm were cut from the specimens on a low speed was and they were further thinned by a mechanical polishing to 0.03 mm. Using punch off tool, a disc in 3 mm in diameter achieved, and final thinning was carried out using a Fischione 1050 low-angle ion milling, operating at 3–5 kV, and ion current of 50 micro amperes and a sample inclination of 10◦ to the ion beam. The mechanical properties of the friction stir welded materials were characterized through microhardness measurements. Microhardness was measured at the centre of the cross section of the joints through Vickers microhardness tester (Future-Tech FM-800, Tokyo, Japan) with the load of 2 N. Tensile tests were performed on specimens cut through electro discharge machining with the centre of the cross section corresponding to the centre of the weld line as shown in Fig. 2. The specimens for uniaxial tensile tests were conducted according to ASTM E8 for small size specimens, with a gauge length of 6.4 mm, 25 mm overall length and 4 mm thickness. The tensile tests on SPD samples were conducted at room temperature with initial strain rate of 10^{-4} s^{-1} using a Zwick/Roell standard testing machine. The more detail about hardness measurement and tensile test are given in our previous papers [13,26,27,33,48,49].

3-points bending tests (Zwick Roell 100 kN) were performed on rectangular specimens schematically indicated in Fig. 2 (in red). The specimens were cut through electro discharge machining in order to have the central section of the rectangle in the same position of the weld line. The samples for the bending tests measured 16*40 mm2 in section and 4 mm in thickness. Cyclic tests were performed in stress-controlled and strain-controlled modes. Specimens were tested in bending by employing a Zwick/Roell standard testing machine. Specimens had the same dimensions as the previous ones. Stress controlled tests were performed at selected percentages of the Yield strength selected after performing the monotonic bending tests. Strain-controlled tests were performed at different levels of the maximum punch stroke (0.3, 0.6, 0.9 1.2, 1.5, 1.8, 2.1, 2.4, 2.7, 3 mm and so on up to a maximum of 4.5 mm).

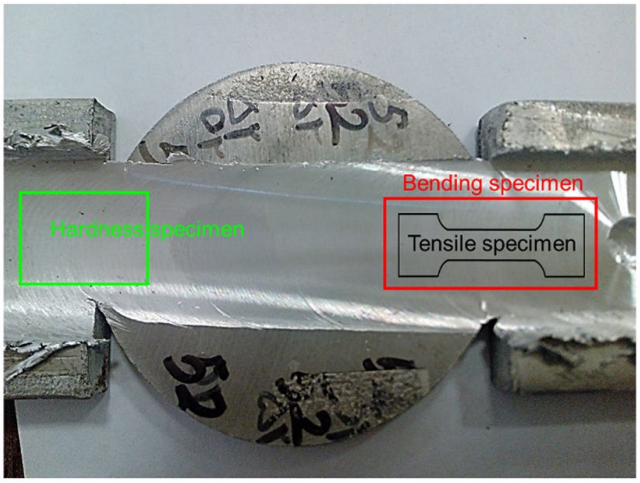

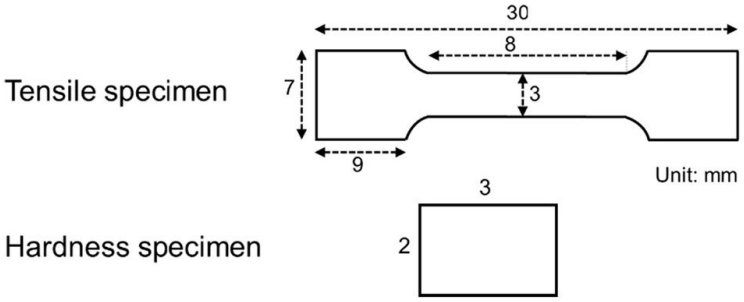

Fig. 2. Schematic of the tensile specimen (black), of the bending specimen (red) and of microhardness specimens (green). (For interpretation of the references to colour in this figure legend, the reader is referred to the web version of this article).

3. Results

The microstructure of the composite at different magnifications after spark plasma sintering is shown in Fig. 3. When the SPS process is conducted, the developed electric potential of the aluminium particles due to the presence of non-conductive ceramic particles can crack the oxide layer. It develops the direct contact between metal particles with a very small porosity presence. These results were consistent with the results reported in [3,26,27,47].

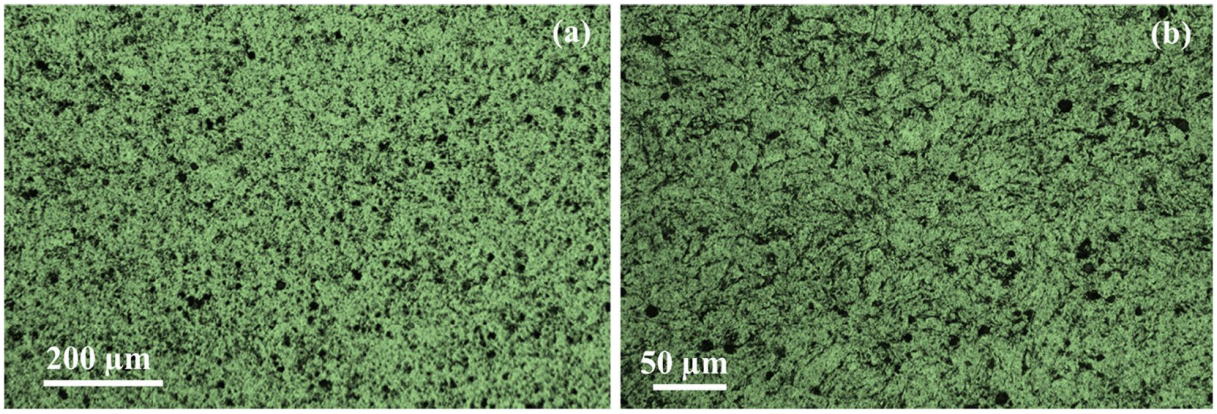

Fig. 3. Microstructure of the studied composite after spark plasma sintering at different magnifications.

The Alumina particles in the range of nano to micron size are depicted with a higher magnified SEM image of the sintered specimen in Fig. 4. The agglomerates of Alumina with large content of nanoparticles are visible as the lighter area in the SEM image (Fig. 4a,c). Its presence is visible in the metal grain boundaries (Fig. 4b). The microscopic Alumina particles appear uniformly distributed. Otherwise, the nanometric particles are distributed along the grain boundaries and inside the grains (Fig. 4c,d).

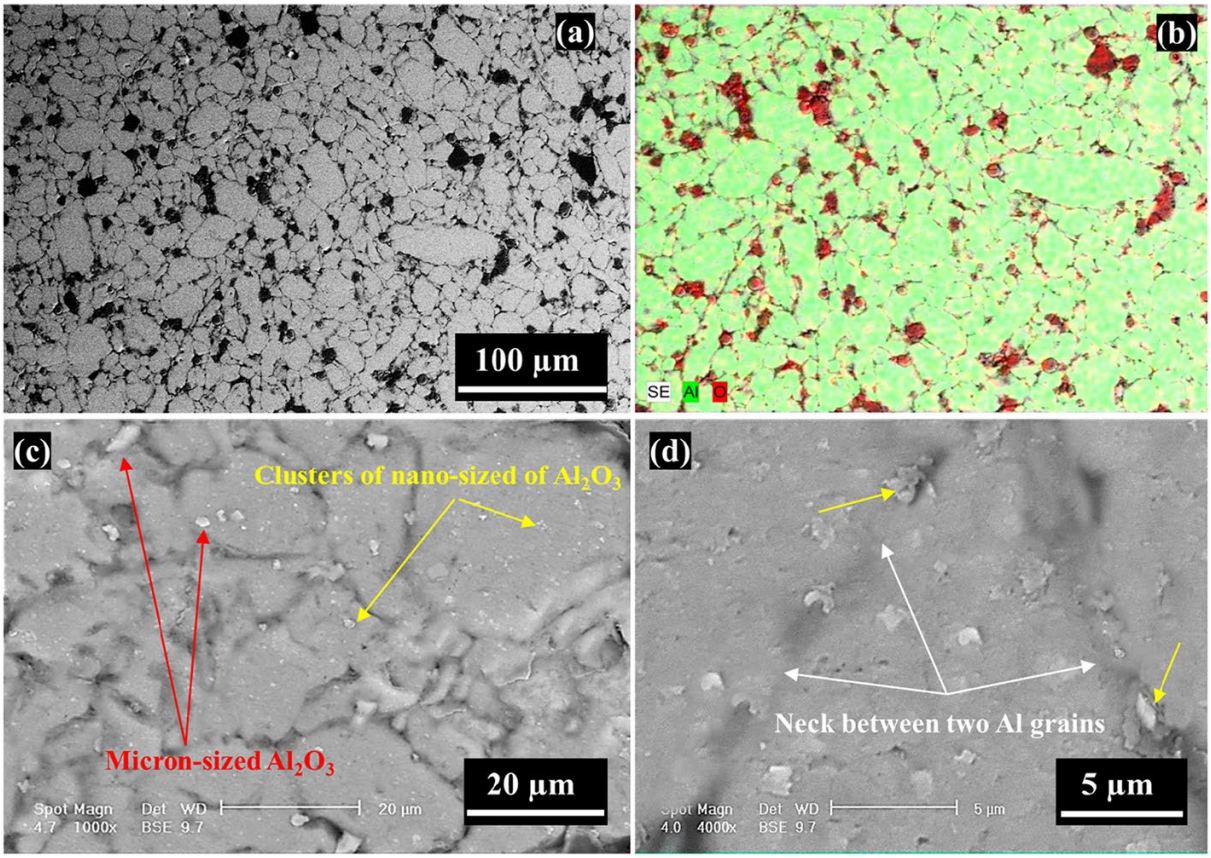

Fig. 4. SEM microstructure of the composite after SPS a); showing the distribution of microscopic and agglomerated nanoscopic Alumina particles b); clustering of nanoparticles at particles necks and inside the different grains c,d).

The distribution is revealed by the X-ray maps as shown in Fig. 5. The occurrence of nanoparticles greatly increases the work hardening rate of Al-matrix. In addition, it enhances the grain refining process. From the X-ray map, it is evident that the presence of the aluminium and aluminium oxide is traced in all the samples. Aluminium carbides are absent in all the samples which are shown in Fig. 5. The X-ray map shows the larger Al peak with smaller Alumina The peaks intensity is compared before and after the sintering process. When the intensity is observed, the peak broadening is found due to the rise of the nanoparticle. Al-2n8mAlumina crystallite size decreases from 82 nm to 46 nm. On contrary, the rise of nanoparticles leads to the hard agglomerates development. Further, it hinders the local plastic deformation of Al particles. It leads to the formation of stains of Alumina nanoparticles on the Al matrix.

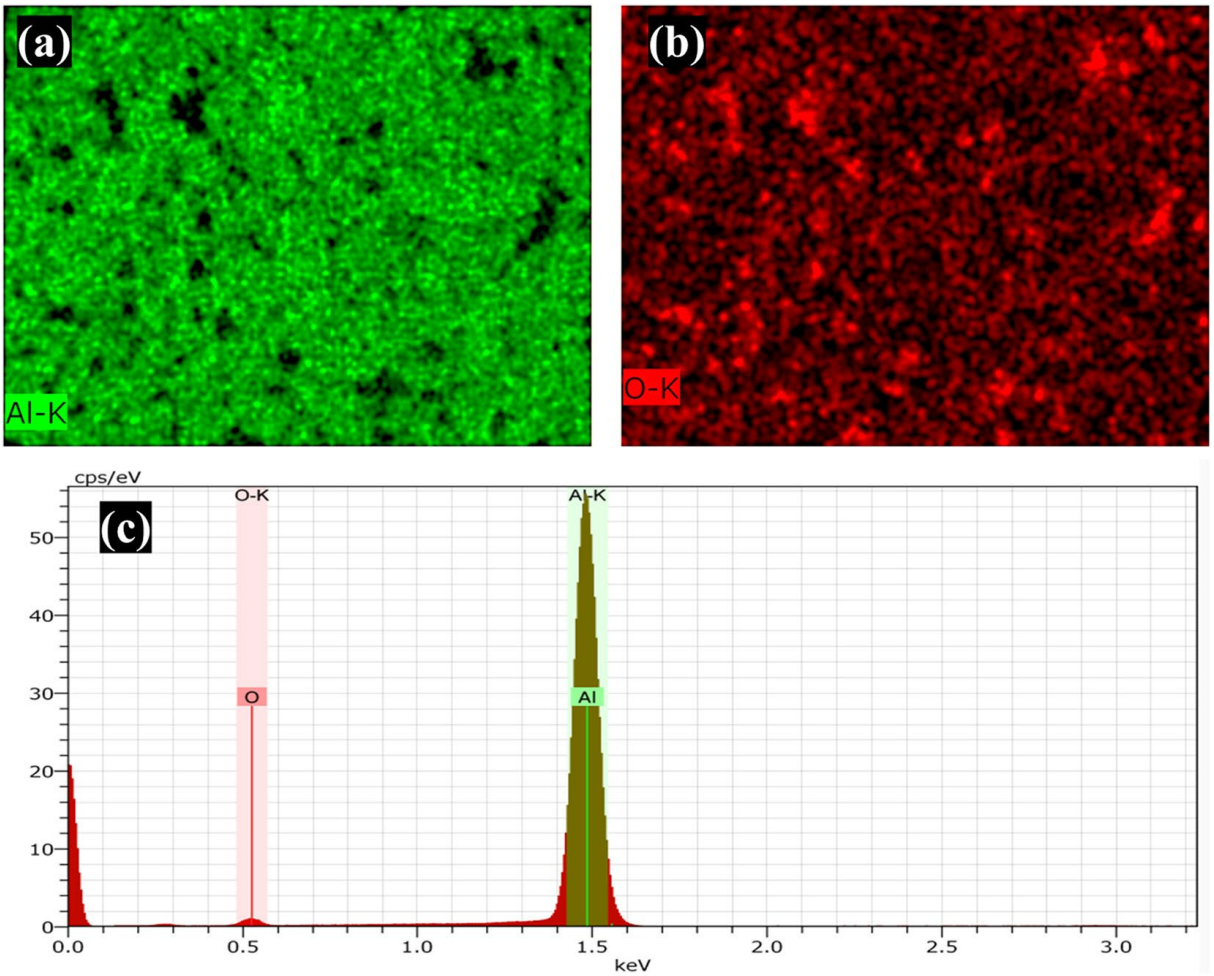

Fig. 5. EDS maps belonging to the analyses of the SEM images shown in Fig. 4; the aluminium and oxygen maps are shown in a) and b); the EDS spectrum is shown in c).

The samples were friction stir welded to pure aluminium sheets and the aspect for selected conditions is shown in Fig. 6. Top-view of the all the welded/processed surfaces appear without the presence of defects, large voids and crack as previously reported by [27,48]. However, at lower ratios of rotating speed to travel speed (lower heat input), some surface inhomogeneities appeared (their images are not given), while in higher input heat caused by higher ratio of rotating speed to travel speed, the appearance of welded zone is so much better without any type of defects. The investigation of the forces acting on the tool is basic to understanding the nature of the material at the processing time.

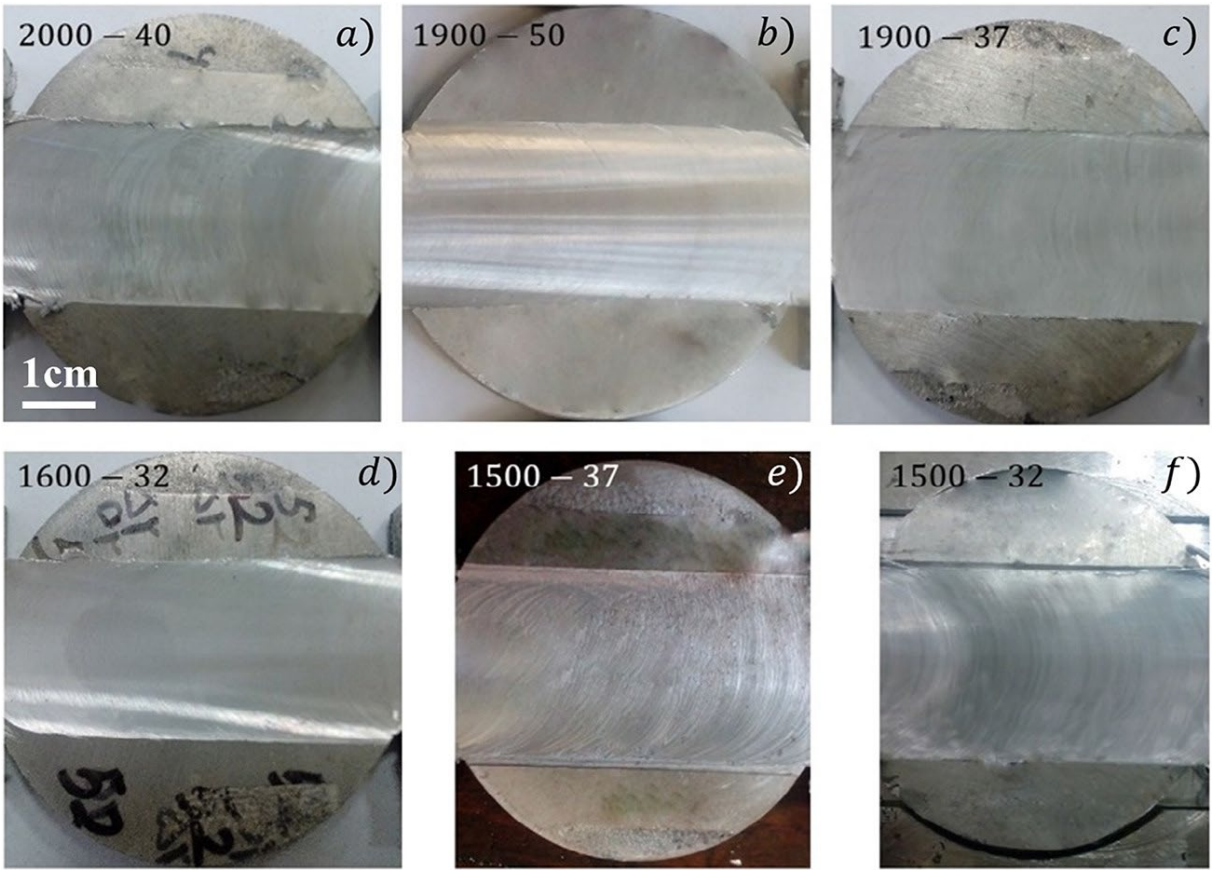

Fig. 6. Aspect of FSWed samples after joining at different processing parameters showing the surface aspect of the welds; 2000 RPM-40 mm/min a), 1900 RPM-50 mm/min b), 1900 RPM-37 mm/min c), 1600 RPM-32 mm/min d), 1500 RPM-37 mm/min e) and 1500 RPM-32 mm/min f).

The travel speed and the rotating speed recorded are mentioned in Fig. 7. The mentioned values refer to the systematic conditions as a function of the pitch revolution. In general, the heat generation is decided by the coefficient of friction, speed of rotation and movement and moving direction. Particularly, the rotation and moving speed raise the heat input [21,48,50].

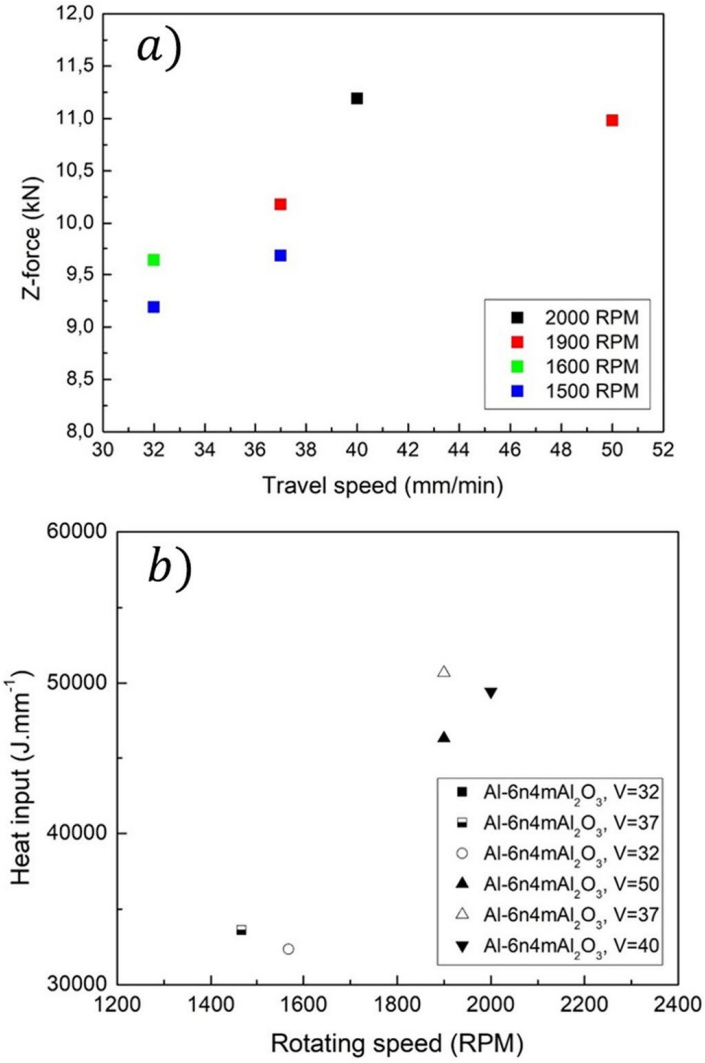

Fig. 7. Force acting on the tool main axis during friction stir welding performed at different processing parameters a); corresponding heat input provided to the welding material b).

It is well-known that microstructural evolution during FSW is due to the heat input provided during processing. Heat input (HI) was calculated through Eq. 1.

$$HI = \frac{2\pi}{3} \times \mu \times P \times W \times S \times R \quad (1)$$

m is the local coefficient of friction; W and V, rotation and travelling speeds, respectively; P, axial force; R, shoulder radius.

When the revolutionary pitch is raised to 1900 rpm of the rotating speed, the force is increased. At 2000 RPM, the force is found to be decreased in the samples taken for study. The friction of the tool against the material in addition to the non-elastic deformation raises the temperature in the friction stirred material. The temperature difference of 0.6–0.9 is developed by the movement and rotating speed of the tool which melts the material [51]. The effect of the produced heat is increased to 50% more based on the process parameters. At the start of the experiment, the temperature of the material is low. Its yield strength is high. Higher force values at the initial stage led to tool penetration. The force in the z-direction (Fz) is induced by the softening material when the tool penetration is complete before the travel movement started. When the force development based on the time is examined, the composite having nanoparticles of 4% increases the Z forces from the nanoparticles of 6%. The Fz

forces decreased when the Alumina presence is 2%. At the same time, the pitch of revolution lowers the Fz for the 8% microsized particle of the sample. It is the result of softening of the material.

The microstructure of the nugget zone of the welds for the different employed processing parameters is shown in Fig. 8. The particles are uniformly distributed which resembles nuggets. The presence of crack is negligible. The presence of porosity, voids are greatly decreased in comparison with the sintering.

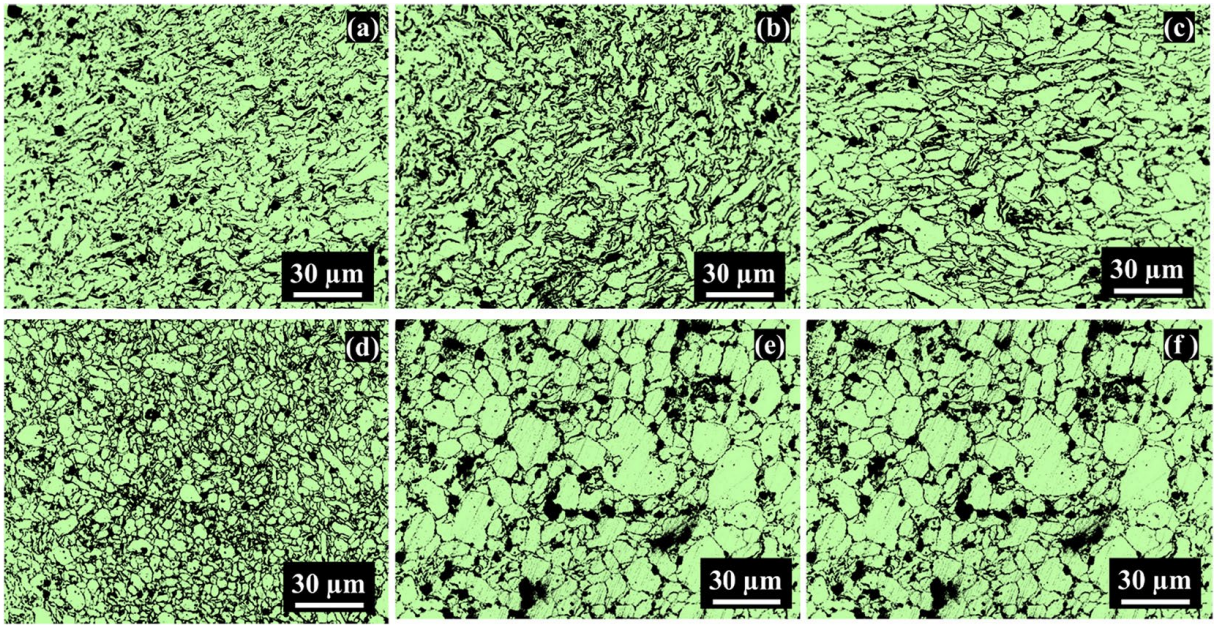

Fig. 8. Nugget zone microstructure, from the top-left 1500 RPM-32 mm/min a), 1500 RPM-37 mm/min b), 1600 RPM-32 mm/min c), 1900 RPM-37 mm/min d), 1900 RPM-50 mm/min e), 2000 RPM-40 mm/min f).

The summary of the mean grain size and the mean aspect ratio per each condition is listed in Table 2.

Table 2
Mean grain size and aspect ratio for the different welding conditions.

Rotating speed (RPM)	Travel speed (mm/min)	Mean grain size (mm)	Aspect ratio
2000	40	12 ±4	1.12
1900	50	10 ±4	1.17
1900	37	13 ±8	1.28
1600	32	4 ±2	1.14
1500	37	9 ±3	1.16
1500	32	12 ±2	2

For the lowest rotating speed at 32 mm/min, the material appears as mixed with few recrystallized grains, then by increasing both rotating speeds, the materials present remarkable dynamic recrystallization. For rotating speeds of 1900 and 2000 RPM, a remarkable grain growth phenomenon can be underlined. Macro- and micro structure observations demonstrated that with decreasing heat input, (smaller W/V), the grain refinement became more distinguishable. Comparing OM images for all the FSW processing conditions with SEM images of ZS regions, the tentative conclusion can be

drawn that increasing the rotation rate from 1500 to 2000 RPM and/or decreasing the traverse speed from 50 to 32 mm/ min reduced the area fraction of the SZ and TMAZ at the expense of a larger HAZ. As a matter of fact, by observing the microhardness profile for all the studied welds this trend is confirmed (Fig. 9). The microhardness profile for all the studied conditions is shown in Fig. 9. The microhardness profiles were described from measurements performed at the centre of the weld cross-section. The highest values are experienced by those welds presenting a more recrystallized microstructure. Also, the welds performed at 2000 RPM show a medium-high hardness, this is believed to be due to the increased microscopic Alumina particles fracture as the rotating speed increases. Obviously, the stir zone is harder than the base metal due to the grain refinement and there also appears to be more uniformly Alumina dispersoids distribution in the welded regions of the aluminium matrix. In addition, by a close look at the inhomogeneity degree of hardness profiles, it can be inferred that the degree of non-homogeneity likely depends on the FSW processing parameters. The results indicates that higher hardness values also attaind when lower heat inputs are produced. These finding are according to the results reported by [31,48].

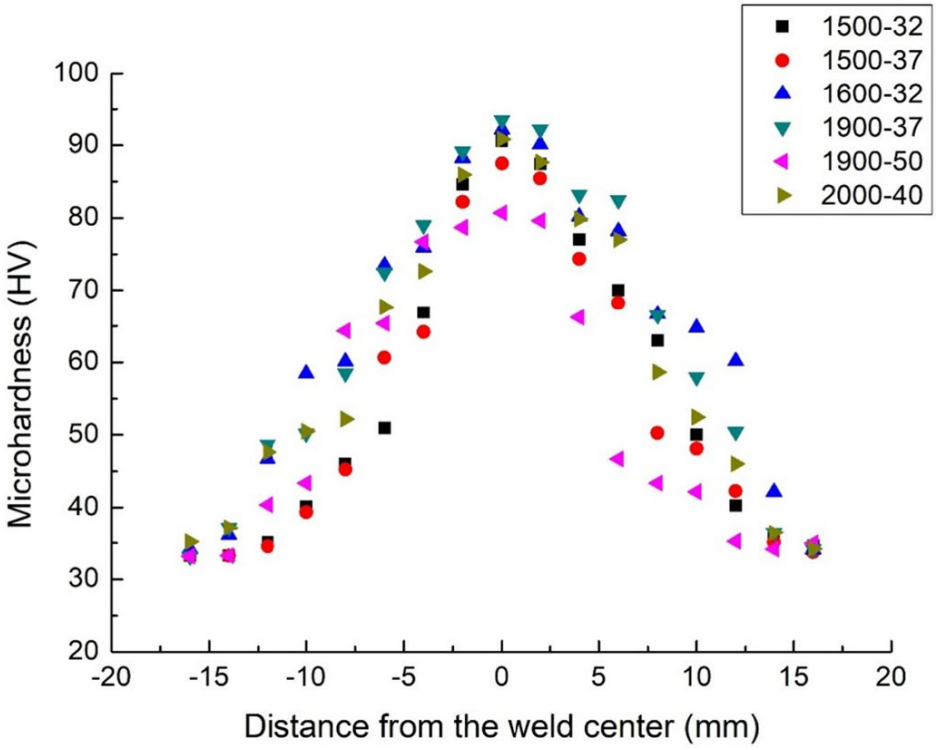

Fig. 9. Microhardness profile for the different employed processing parameters.

The tensile specimens for the studied joints are shown in Fig. 10.

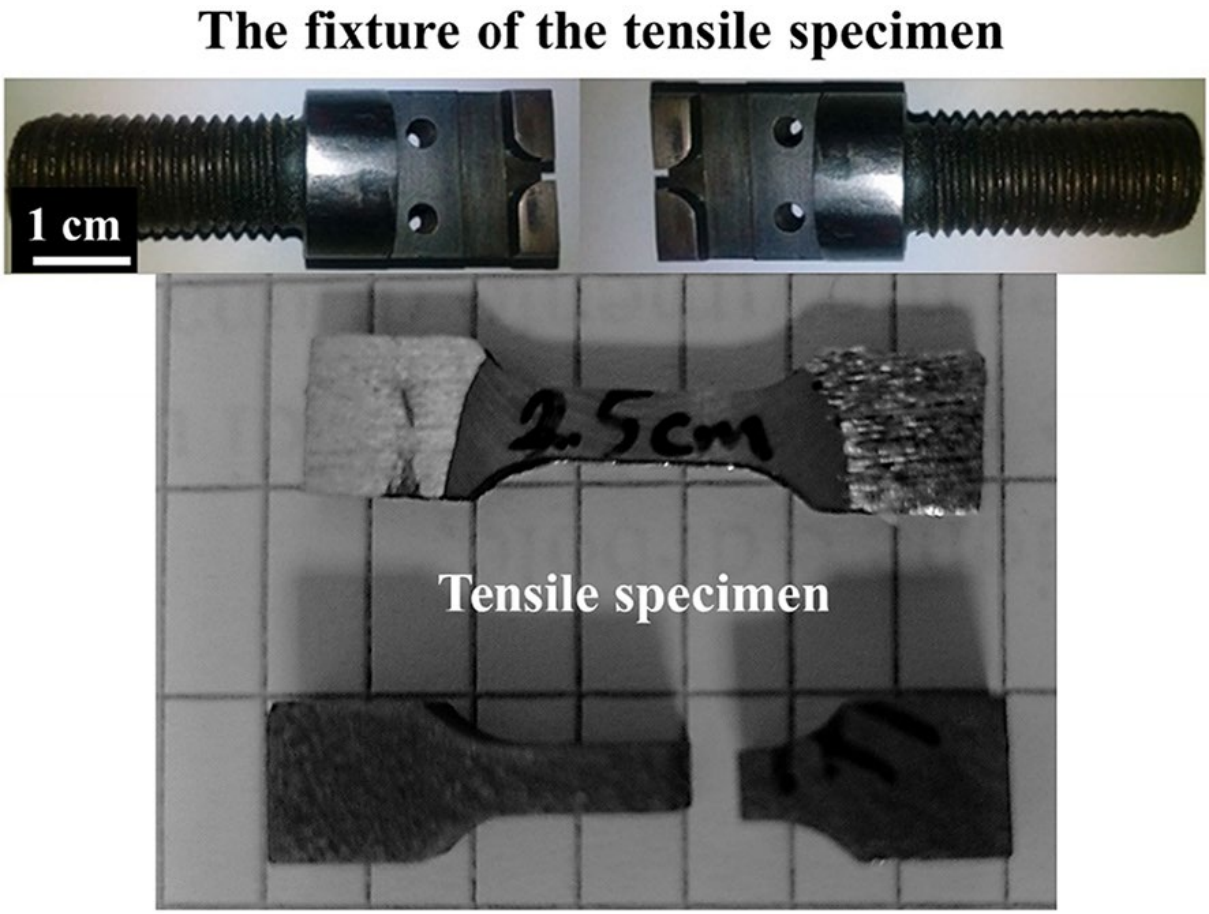

Fig. 10. The tensile test's fixture and tensile specimens to evaluate the recrystallized materials properties.

The tensile tests performed on the specimens shown in Fig. 10 show the same trend on the microhardness ones revealing the effect of microstructure on the behaviour of the material. The tensile curves for selected conditions are shown in Fig. 11. The weld performed at 1600RPM and 32 mm/min presents the highest tensile strength, the grain growth leads to increased ductility (1900 RPM samples) while the lowest rotating speed leads to the worst tensile properties because of the non-complete nugget recrystallization during welding. As a matter of fact, the heat input or W/V ratio strongly affected the mechanical properties especially tensile properties of the welded materials. Lower heat input (W = 1500 RPM and V = 32 mm/min) yielded lower yield strength and tensile strength, while at higher heat input, the loss of the tensile strength improved remarkably without significant loss in the ductility.

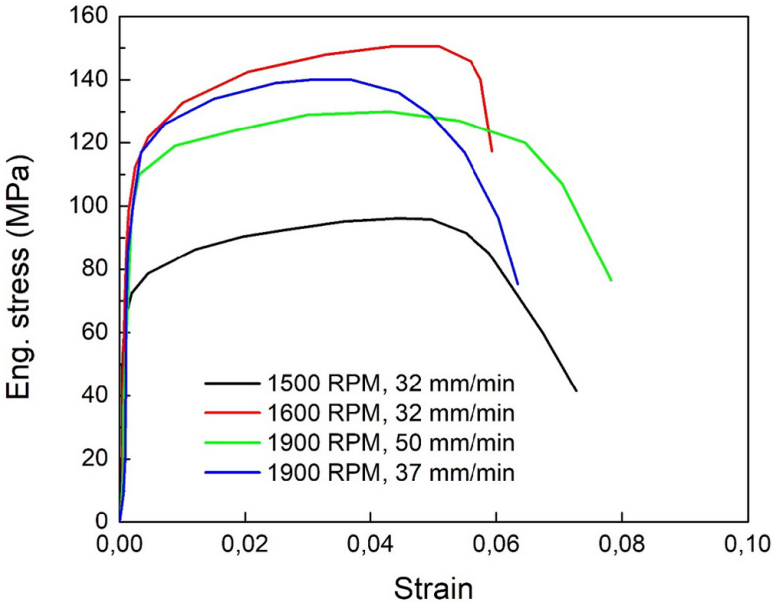

Fig. 11. Tensile curves for selected friction stir welding conditions.

The corresponding 3-point bending stress-strain curves are shown in Fig. 12. The weld performed at 1600 RPM, 32 mm/min and 1900 RPM, 37 mm/min show the highest strength and ductility in bending.

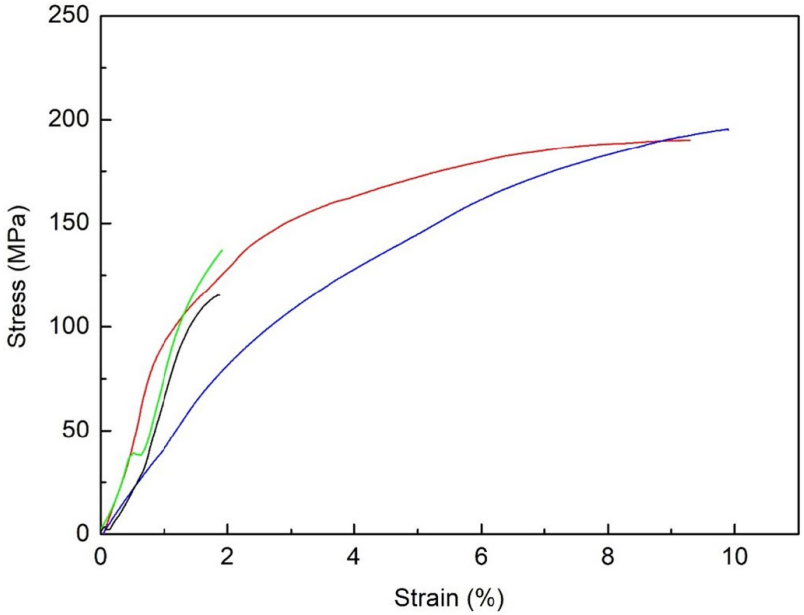

Fig. 12. Stress-strain curves belonging to 3 point bending tests performed on the studied joints.

The summary of the cyclic 3-point bending behaviour of the studied joints is shown in Fig. 13. As it can be observed by Fig. 13, those joints performed at 1500 RPM have a very brittle and anticipated fracture concerning those joints performed at an increased toll rotation speed. This acts in the case of cyclic bending tests performed at fixed maximum vertical stroke. It can be highlighted that joints performed at 1500 RPM and 32 mm/min brakes after 0,6 mm of cyclic bending reveal the very brittle nature of this weld. The joints performed at 1600 RPM and 32 mm/min sow an increased maximum load as increasing the maximum vertical displacement up to 3.6 mm of maximum stroke, after this, the joints fail. These frictions stir welds are those showing the maximum strength at the same deformation level. Those joints friction stir welded at 1900 RPM and 50 and 37 mm/min show very similar behaviour. The joint performed at 1900 RPM and 37 mm/min shows an increased hardening as the maximum vertical

displacement increases with a lower maximum load at the same displacement level up to 1.5 mm and then with a higher maximum load at the same displacement level as the maximum stroke during bending increases.

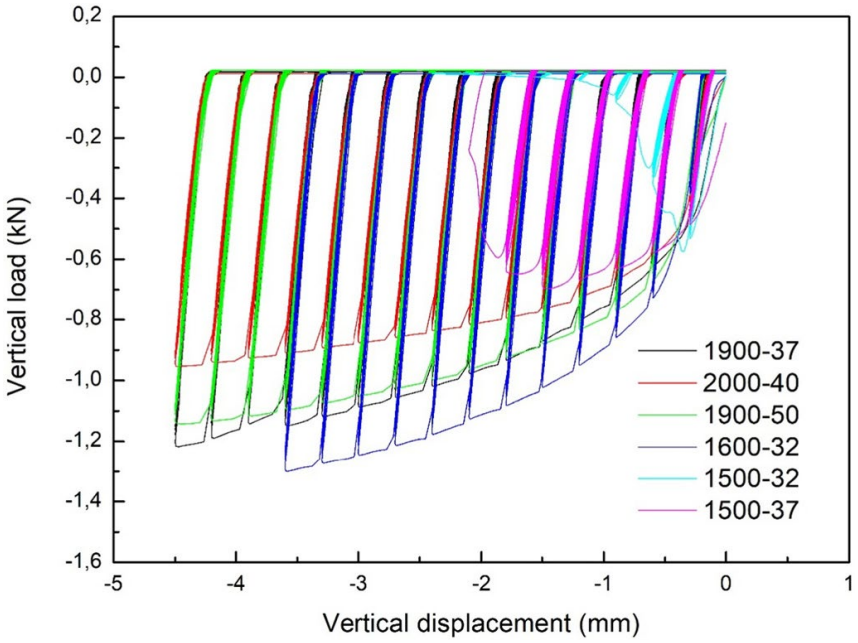

Fig. 13. 3-point bending fatigue curves performed on the studied joints.

These curves refer to tests performed at different levels of the maximum stroke by recording the corresponding load cycle by cycle. In a summary, the maximum vertical load as a function of the vertical displacement for selected joints is shown in Fig. 14.

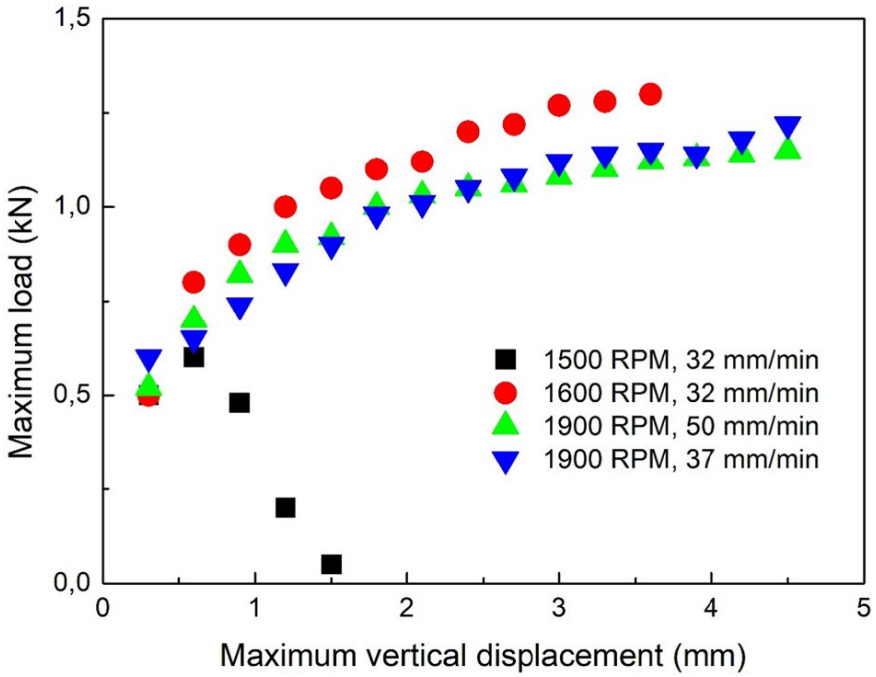

Fig. 14. Maximum load versus maximum imposed vertical displacement for the cyclically loaded joints in 3 points bending.

The fatigue bending curves performed with R = 0.1 in stress control mode for the selected joints are shown in Fig. 15. In stress control mode, it seems that the best fatigue performances are experienced

by the joint performed at 1900 RPM and 37 mm/min. Here, the balancing between the mixing due to the increased rotating speed balances the increased grain size due to the increased heating producing more sound friction stir welded joints.

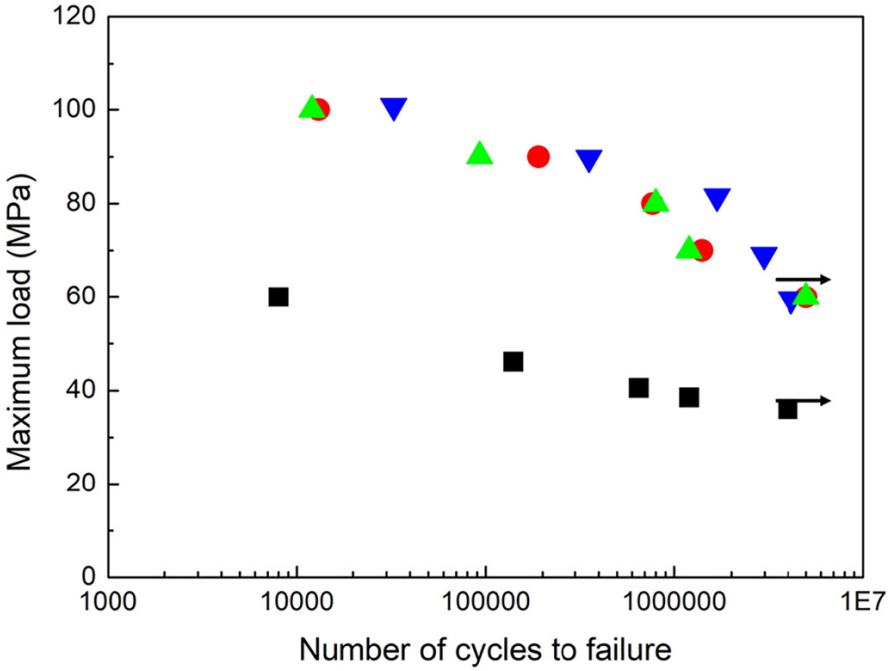

Fig. 15. Fatigue bending curves for the studied joints.

The fracture surfaces of the joints after fatigue tests are shown in Fig. 16. The microstructure characterisation of fractured surfaces of the Al composite with the varied ratio of the addition of the nano-micro sized Alumina. It reveals that the addition of two different sized Alumina increases the strength with the decrease in ductility. The poor bonding of the Alumina with nano al matrix leads to the fracture at the FSW process. The processing condition increase brittleness with minimum non-elastic deformation. The microporosity nucleation occurrence is found which is the result of crack formation between the Alumina particle and Al matrix. The growth of microporosity as a result of tensile force application leads to coalescence which leads to fracture.

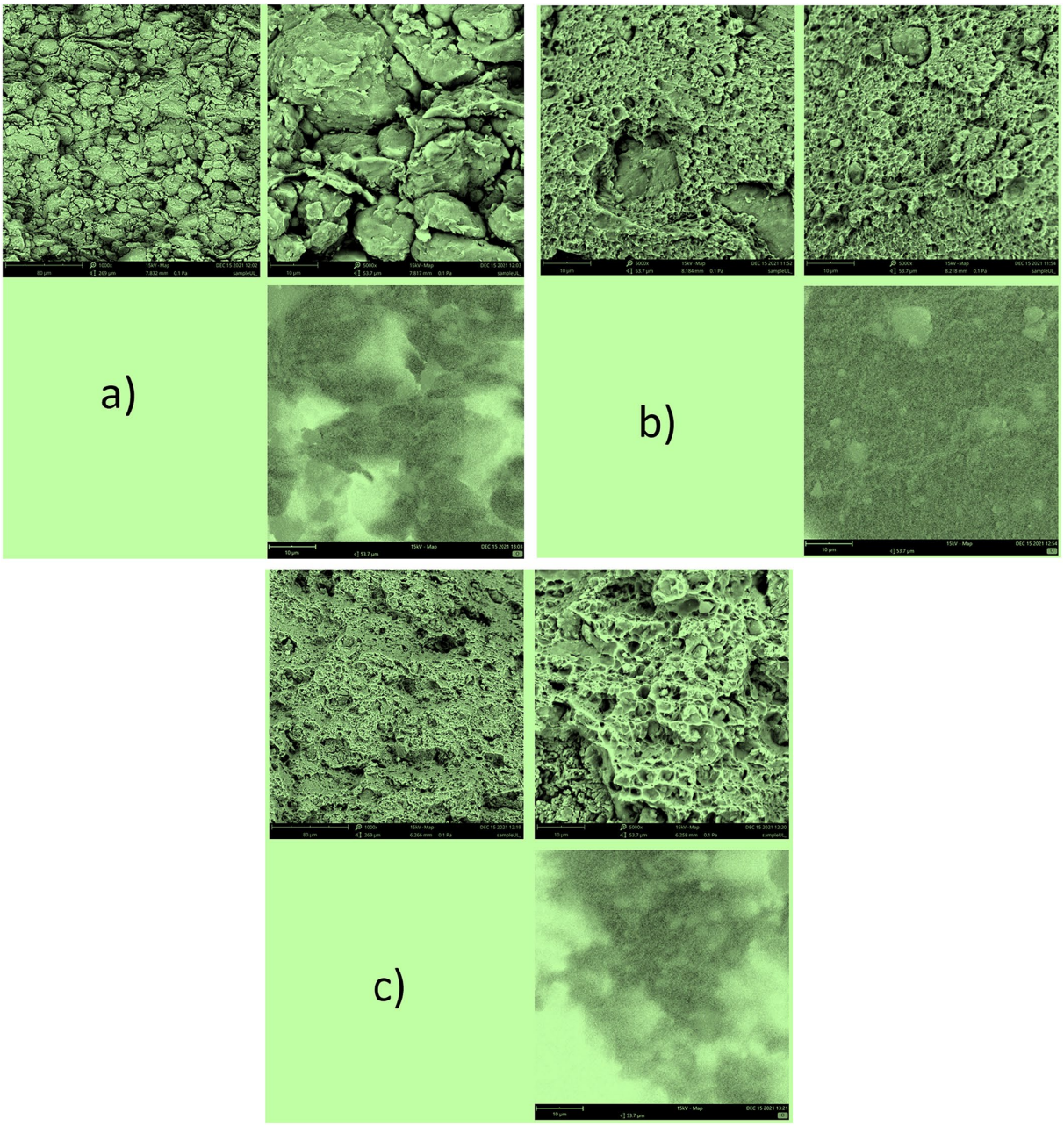

Fig. 16. Fracture surface aspect of the joints after bending fatigue tests friction stir welded at 1500 RPM and 32 mm/min a); 1600 RPM and 32 mm/min b); 1900 RPM and 37 mm/min c).

4. Discussion

The contact zone of the adjacent Al powder particles has been raised to 1000 times if uses SPS process as a consolidation step [52]. It is the result of the generated spark which raises the local temperature of the contact point. Moreover, the applied pressure causes the formation of the neck at the particle's contact point. At the same time, the oxide layer thickness, pressure for compacting and the size of the particle affect the current supply for sintering [48,52].

The material porosity was measured the ASTMB962–14 and it resulted in 96.78%. The crystallite size resulted in 40 nm. This is one of the reasons why this particular composition was chosen for this study. Among many combinations of nano- and micro-sized Alumina particles, the selected combination allowed for obtaining the finest crystallite size mbut non-optimal material density [27]. Anyway, it is

demonstrated that this last property can be largely improved through the further friction stir processing, so, it was selected 6% of nanoparticles and 4% of microparticles increased mechanical properties thanks to the microstructural refinement effect [39]. Nanoparticles clustering during densification leads to nanovoids increase but increased grain refinement at the employed pressure, temperature and applied pulsed current. The crystallite size reduction is due to the increased strain in the ductile matrix as the nanoparticle's volume increases at the same total reinforcing volume [52]. The formed agglomeration as a result of nanoparticles increases decreases the mechanical properties of the material. It is the result of the initial force of friction stirred process of the Alumina reinforced Al nanocomposites.

As expected, the surface aspect is very sensitive to the processing parameters employed during welding. The welds joined at 1600 RPM and 32 mm/min as well as those joined at 1900 RPM show the less presence of surface tool tracks (Fig. 17).

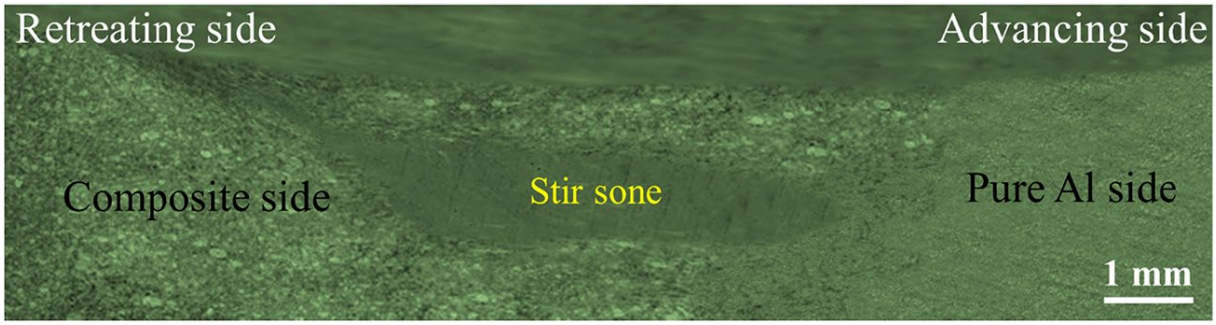

Fig. 17. Typical cross-section of FSW welds of Al-4n6mAlumina at 1600 RPM, 32 mm/min.

As the rotating speed decreases (1500 RPM) or the advancing speed increases (50 mm/min), the tracks start to be more evident. To evaluate this, we performed also the measurement of the force on the tool during welding. Low heat input generates insufficient metal flow during stirring. So, low peak temperature and consequent cooling rate lead to nonproper conditions for dynamic recrystallization (DRX) and continuous dynamic recrystallization (CDRX) to take place. On the other hand, higher heat input allows for increased material turbulence around the tool, with increased severe plastic deformation and consequent optimal plasticization [19]. So, improved plasticization leads to more refined grain size thanks to the provided severe plastic deformation and improved distribution of the nanosized reinforcing Alumina particles. It is immediately clear how the heat input governs the dynamic recrystallization phenomenon during severe plastic deformation.

The density of the Al-4n6mAlumina increases to 96.6%. It occurs with a rising ratio of nano to micro-sized Alumina. When the ratio increases further, the density decreases. It is the result of sintering parameters and characteristics of microstructure. The sintering parameters such as heating rate, current supply and the sintering pressure affect the density of the sample preparation. The density of the sample is further affected as the Al and Alumina are highly sensitive to the sintering temperature and pressure [53].

The sintering pressure enhances the neck formation between the Al particles and densification regardless of low temperature. At high temperatures, the heat transfer rate helps to achieve a dense sample in a shorter time. In addition, pure Al is more reactive to the deformation mechanism than ceramics. The grain boundary and the volume diffusion cause the densification of the mixed powders. The surface diffusion favours densification when the mixed powder is introduced to a high temperature [39]. It applies to the SPS process as the surface of the particles is activated by the generated spark which hinders the neck formation. It ultimately increases the density. At the same

time, the further addition of Alumina decreases the density. It is the result of agglomeration and the compressibility of non-deformable nanoparticles [54,55]. On contrary, the addition of the nanoparticles will reduce the compressibility. It is because the nanoparticles possess a higher specific surface area in comparison with the microparticles. The addition of Alumina nanoparticles with aluminium matrix increases the total specific surface area which increases the interaction between the nanoparticles. Further, it enhances the interparticle distance in comparison with the theoretical value. The increased interparticle distance causes the agglomeration and its potentiality to form interconnected networks between nanoparticles. These two factors lead to a decrease in densification. In addition, the nano Alumina particles addition rises the composite hardness.

From the obtained values, it is evident that the microhardness increases and then slightly lower with nano-micro sized Alumina particles. Overall, the mechanical properties are affected by the amount of Alumina particles and agglomeration. In addition, the nanoparticles enhance the strengthening mechanisms such as Orowan by-pass, Hall-Petch effect and dislocation strengthening [56]. The Alumina particles of micro-size are distributed at the grain boundaries. The Alumina particles of the nano side are found in the grain interiors (Fig. 17). Thanks to the presence Alumina dispersoids both in grain interior (nanosized ones) and at grain boundaries (microsized ones), a significant stability of microstructure is happened. Obviously that the distribution of Alumina dispersoids dependent FSW processing parameters which in turn severely affects the Orowan strengthening, load transfer strengthening as well as thermal expansion coefficient [31,57]. The agglomeration is reduced when the Alumina nanoparticles are lesser than 4 wt%. The interparticle distance of the Alumina particles in the Al matrix is lesser than the agglomerated substance which induces the particle dislocation interaction [58]. It is reported that the stronger diffusion bonds and the structural integrity enhance the tensile strength and microhardness of the composite after SPS [29,49,59]. An increase in pores and interparticle distance is found due to the high ratio of nano to micro-sized Alumina particles. It leads to the weakening of the material [60–62].

From one side, the grain boundaries generated by CDRX are relatively anchored by Zenner pinning pressure [63]. From another side, the pre-stored energy caused by ball milling and higher rotating speed of FSW tools, provides an ideal condition to occur the DRX and grain growth. In addition, the settle of nanosized Alumina particles in the grain interior strongly affect the glide dislocation in the grain interior, and consequently increase the proportion of dislocation strengthening in the SZ regions (Fig. 18).

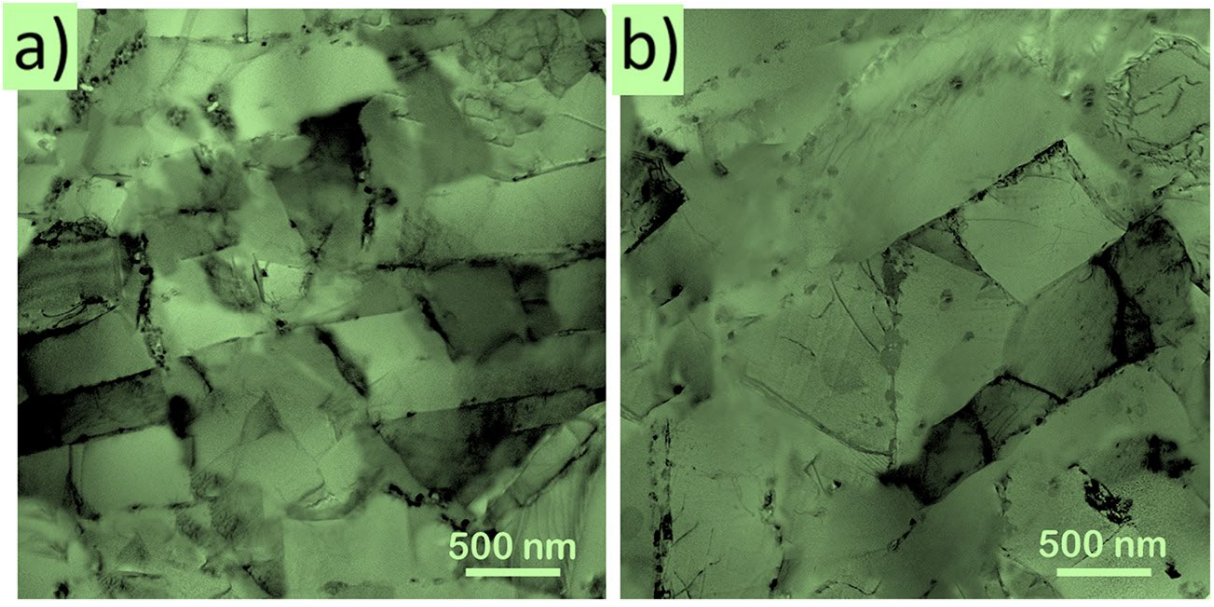

Fig. 18. Bright field TEM image of stir zone in the Al-4n6mAlumina (a) at 1500 RPM, 32 mm/min, and (b) at 1600 RPM, 32 mm/min.

The tensile graph of the composites reveals that the strength of the composites increases at the initial stage. It decreases when the number of nanoparticles goes more than 4 wt%. It reveals that the proposed bimodal particle influences the tensile and yield strength of the composites [47,61]. The distance between the Alumina particles decreases which requires higher energy to move the dislocation for deformation. Thus, the Alumina particles having less than 4 wt% experience higher yield and tensile strength.

The presence of Alumina nanoparticles increases the brittle phase formation along the grain boundaries which increases the tendency of fracture formation at the grain boundaries. A higher occurrence of Alumina agglomerates into the micropores is found. The size and the quantity of the agglomerates increase with the increase in the ratio of nano/micro-sized particles at the grain boundaries of the Al matrix. The higher porosity presence provides the way for crack initiation and embrittlement. By analysing the microstructure, it is evident that the fracture formation is mainly transgranular. In addition, the tensile results confirm that the higher addition of nanoparticles enhances the local ductility. Since pure aluminium has good ductility, the fracture is the result of the microporosity merging. So, the best reinforcing particles distribution and ratio of nano/micro-Alumina particles due to the tool rotation leads to increased mechanical properties in a more pronounced way concerning the decrease of the strength due to grain growth by the Hall-Petch relationship. The rotating tool induces severe plastic deformation and frictional heating of base metal. Which in turn causes that the predominant deformation mode be a simple shear [64]. Such ,deformation state could effectively increase the heat generated and consequently facilitate the occurrence of dynamic recrystallization. Moreover, the addition of bimodal particle sized alumina remarkably enhances the grain refinement, in particular in stir zone during FSW. Furthermore, the presence of Alumina dispersoid effectively cause hindering the grain boundary migration, and subsequent grain growth in the stir zone. In a word, a uniform dispersion of nano-Alumina particle in the grain interior of Al plus some micron-sized Alumina particles at Al grain boundaries significantly hinder the dislocation glide during subsequent cyclic loading.

5. Conclusion

The aluminium-based nanocomposites with the addition of Alumina in different ratios of nano and micro-sized particles are powder metallurgically produced through spark plasma sintering. The produced samples are friction stirred by altering the rotating speed and the travel speed. The results of the microstructure development, the mechanical properties and fatigue behaviour of the nanocomposite revealed that

1. The properties of the FSW processed sample strongly depend on its processing parameters.

2. By analysing the hardness of the friction stirred composites, it is clear that the recrystallization increases concerning the increase in the amount of nano Alumina particles. The recrystallization capability further contributes to the strength of the composite compared to the coarse particles.

3. The particles retaining their original shape indicates that the nanosized particles induce recrystallization which leads to the hard ceramic phase moving throughout the tool with no fracture. In the case of micro-sized particles, uniform flow is found in the material with negligible fracture location.

4. Due to significant grain refinement and the presence of hard Alumina dispersoids, the tensile strength was significantly improved with a loss in the ductility.

5. The higher fatigue strength is strongly dependent the processing parameters, as the best fatigue performances are experienced by the joint performed at 1900 RPM and 37 mm/min.

6. A higher fatigue strength of the bimodal sized Al2O3/Al nanocomposites fabricated through the combination of SPS and FSW due to the uniform presence of nano sized Alumina in the grain interior, as well as micro-sized Alumina at grain boundaries. Former is restricted the dislocation mobility and latter limit the grain boundary migration. It is clear evidence that a smaller percentage addition of micron and nano sized Alumina are effectively increased the fatigue life to a greater extent.

7. Fracture surfaces confirmed also a combined ductile–brittle fracture mode with fine-sized and shallower dimples for the nanocomposite processed at 1900 RPM and 37 mm/min compared to a ductile fracture mode with other processing conditions.

Data availability statement

Data will be available on request to the Corresponding author.

CRediT authorship contribution statement

P. Cavaliere: Conceptualization, Validation, Supervision, Formal analysis, Investigation, Writing – original draft. A. Laska: Formal analysis, Investigation. A. Perrone: Formal analysis, Investigation. G. Blasi: Formal analysis, Investigation. A. Gopinathan: Formal analysis, Investigation. M. Shamanian: Supervision, Formal analysis, Investigation. F. Ashrafizadeh: Supervision, Formal analysis, Investigation.

Declaration of Competing Interest

The authors declare that they have no known competing financial interests or personal relationships that could have appeared to influence the work reported in this paper.

Data availability

Data will be made available on request.

Acknowledgement

This work was performed during the implementation of the project Building-up Centre for advanced materials application of the Slovak Academy of Sciences, ITMS project code 313021T081, supported by Research & Innovation Operational Programme funded by the ERDF.

References

[1] P. Niu, W. Li, C. Yang, Y. Chen, D. Chen, Low cycle fatigue properties of friction stir welded dissimilar 2024-to-7075 aluminum alloy joints, Mater. Sci. Eng. A 832 (2022), 142423.

[2] G. Demeneghi, K. Rodgers, C. Hua Su, W.M. Medders, S. Gorti, R. Wilkerson, Root cause analysis of premature simulated life cycle failure of friction stir welded aluminum 2219, Eng. Fail. Anal. 134 (2022), 106059.

[3] P. Cavaliere, B. Sadeghi, M. Shamanian, F. Ashrafizadeh, Al-based nanocomposites produced via spark plasma sintering: Effect of processing route and reinforcing phases, in: P. Cavaliere (Ed.), Spark Plasma Sintering of Materials: Advances in Processing and Applications, Springer International Publishing, Cham, 2019, pp. 161–190.

[4] A. Borrell, L. Navarro, C.F. Guti´errez-Gonz´alez, C. Alc´azar, M.D. Salvador, R. Moreno, Microstructure and mechanical properties of 4YTZP-SiC composites obtained through colloidal processing and spark plasma sintering, Bolet. Soc. Espa˜n. Cer´am. Vidrio 60 (3) (2021) 175–182.

[5] B. Sadeghi, B. Sadeghian, A. Taherizadeh, A. Laska, P. Cavaliere, A. Gopinathan, Effect of porosity on the Thermo-mechanical behavior of friction-stir-welded spark plasma- sintered aluminum matrix composites with bimodal micro- and nano-sized reinforcing Al2O3 particles, Metals 12 (10) (2022) 1660, https://doi.org/10.3390/ mmet12101660.

[6] K.L. Firestein, A.E. Steinman, I.S. Golovin, J. Cifre, E.A. Obraztsova, A.T. Matveev, mA.M. Kovalskii, O.I. Lebedev, D.V. Shtansky, D. Golberg, Fabrication, characterization, and mechanical properties of spark plasma sintered Al–BNm nanoparticle composites, Mater. Sci. Eng. A 642 (2015) 104–112.

[7] Z.F. Liu, Z.H. Zhang, J.F. Lu, A.V. Korznikov, E. Korznikova, F.C. Wang, Effect of sintering temperature on microstructures and mechanical properties of spark plasma sintered nanocrystalline aluminum, Mater. Des. 64 (2014) 625–630.

[8] B. Sadeghi, A. Shabani, P. Cavaliere, Hot rolling of spark-plasma-sintered pure aluminium, Powder Metall. 61 (4) (2018) 285–292.

[9] C. Wolff, S. Mercier, H. Couque, A. Molinari, Modeling of conventional hot compaction and spark plasma sintering based on modified micromechanical models of porous materials, Mech. Mater. 49 (2012) 72–91.

[10] P. Xue, B.B. Wang, X.H. An, D.R. Ni, B.L. Xiao, Z.Y. Ma, Improved cyclic softening behavior of ultrafine-grained cu with high microstructural stability, Scr. Mater. 166 (2019) 10–14.

[11] A.M.H. Ibrahim, M. Balog, P. Krizik, F. Novy, Y. Cetin, P. Svec Jr., O. Bajana, M. Drienovsky, Partially biodegradable Ti-based composites for load-bearing implants subjected to cyclic loading, 2022.

[12] H. Mughrabi, H.W. H¨oppel, Cyclic deformation and fatigue properties of very finegrained metals and alloys, Int. J. Fatigue 32 (9) (2010) 1413–1427.

[13] B. Sadeghi, B. Sadeghian, A. Taherizadeh, A. Laska, P. Cavaliere, A. Gopinathan, Effect of porosity on the thermo-mechanical behavior of friction-stir-welded sparkplasma- sintered aluminum matrix composites with bimodal micro- and nano-sized reinforcing Al2O3 particles, Metals 12 (10) (2022) 1660.

[14] B. Sadeghi, M. Shamanian, F. Ashrafizadeh, P. Cavaliere, Effect of processing parameters on microstructural and mechanical properties of aluminum–SiO2 nanocomposites produced by spark plasma sintering, Int. J. Mater. Res. 109 (5) (2018) 422–430, https://doi.org/10.3139/146.111625.

[15] B. Sadeghi, M. Shamanian, P. Cavaliere, F. Ashrafizadeh, Effect of processing parameters on the microstructural and mechanical properties of aluminum–carbon nanotube composites produced by spark plasma sintering, Int. J. Mater. Res. 109 (10) (2018) 900–909.

[16] R. Senthilkumar, N. Arunkumar, M.M. Hussian, A comparative study on low cycle fatigue behaviour of nano and micro Al2O3 reinforced AA2014 particulate hybrid composites, Results Phys. 5 (2015) 273–280.

[17] A.M. Hassan, M. Almomani, T. Qasim, A. Ghaithan, Effect of processing parameters on friction stir welded aluminum matrix composites Wear behavior, Mater. Manuf. Process. 27 (12) (2012) 1419–1423.

[18] W. Yuan, R.S. Mishra, S. Webb, Y.L. Chen, B. Carlson, D.R. Herling, G.J. Grant, Effect of tool design and process parameters on properties of Al alloy 6016 friction stir spot welds, J. Mater. Process. Technol. 211 (6) (2011) 972–977.

[19] G. Minak, L. Ceschini, I. Boromei, M. Ponte, Fatigue properties of friction stir welded particulate reinforced aluminium matrix composites, Int. J. Fatigue 32 (1) (2010) 218–226.

[20] P. Cavaliere, A. Squillace, F. Panella, Effect of welding parameters on mechanical and microstructural properties of AA6082 joints produced by friction stir welding, J. Mater. Process. Technol. 200 (1–3) (2008) 364–372.

[21] P. Cavaliere, G. Campanile, F. Panella, A. Squillace, Effect of welding parameters on mechanical and microstructural properties of AA6056 joints produced by friction stir welding, J. Mater. Process. Technol. 180 (1–3) (2006) 263–270.

[22] Z.Y. Ma, S.C. Tjong, S.X. Li, Static and cyclic creep behavior of in situTiB2 particulate reinforced aluminum composite, J. Mater. Res. 14 (12) (1999) 4541–4550.

[23] N.K. Babu, K. Kallip, M. Leparoux, K.A. AlOgab, X. Maeder, Y.A.R. Dasilva, Influence of microstructure and strengthening mechanism of AlMg5–Al2O3 nanocomposites prepared via spark plasma sintering, Mater. Des. 95 (2016) 534–544.

[24] B. Sadeghi, P. Cavaliere, M. Balog, C.I. Pruncu, A. Shabani, Microstructure dependent dislocation density evolution in micro-macro rolled Al2O3/Al laminated composite, Mater. Sci. Eng. A 830 (2022), 142317.

[25] H. Izadi, A. Nolting, C. Munro, D. Bishop, K. Plucknett, A. Gerlich, Friction stir processing of Al/SiC composites fabricated by powder metallurgy, J. Mater. Process. Technol. 213 (11) (2013) 1900–1907.

[26] B. Sadeghi, M. Shamanian, P. Cavaliere, F. Ashrafizadeh, M. Sanayei, J.A. Szpunar, Microstructural and mechanical behavior of bimodal reinforced Al-based composites produced by spark plasma sintering and FSP, Int. J. Adv. Manuf. Technol. 94 (9–12) (2018) 3903–3916.

[27] B. Sadeghi, M. Shamanian, F. Ashrafizadeh, P. Cavaliere, A. Rizzo, Friction stir processing of spark plasma sintered aluminum matrix composites with bimodal micro- and nano-sized reinforcing Al 2 O 3 particles, J. Manuf. Process. 32 (2018) 412–424.

[28] J. Guo, J. Liu, C. Sun, S. Maleksaeedi, G. Bi, M. Tan, J. Wei, Effects of nano-Al2O3 particle addition on grain structure evolution and mechanical behaviour of friction-stir-processed Al, Mater. Sci. Eng. A 602 (2014) 143–149.

[29] P. Cavaliere, F. Jahantigh, A. Shabani, B. Sadeghi, Influence of SiO2 nanoparticles on the microstructure and mechanical properties of Al matrix nanocomposites fabricated by spark plasma sintering, Compos. Part B 146 (2018) 60–68.

[30] Q. Zhang, B. Xiao, Q. Wang, Z. Ma, In situ Al3Ti and Al2O3 nanoparticles reinforced Al composites produced by friction stir processing in an Al-TiO2 system, Mater. Lett. 65 (13) (2011) 2070–2072.

[31] F. Khodabakhshi, H. Ghasemi Yazdabadi, A.H. Kokabi, A. Simchi, Friction stir welding of a P/M Al–Al2O3 nanocomposite: microstructure and mechanical properties, Mater. Sci. Eng. A 585 (2013) 222–232.

[32] K. Kalaiselvan, N. Murugan, Role of friction stir welding parameters on tensile strength of AA6061–B4C composite joints, Trans. Nonferrous Metals Soc. China 23 (3) (2013) 616–624.

[33] B. Sadeghi, P. Cavaliere, M. Nosko, V. Trembo˘Sov´A, ˘S. Nagy, Hot deformation behaviour of bimodal sized Al2O3/Al nanocomposites fabricated by spark plasma sintering, J. Microsc. 281 (1) (2021) 28–45.

[34] B. Sadeghi, M. Shamanian, F. Ashrafizadeh, P. Cavaliere, A. Rizzo, Influence of Al2O3 nanoparticles on microstructure and strengthening mechanism of Al-based nanocomposites produced via spark plasma sintering, J. Mater. Eng. Perform. 26 (6) (2017) 2928–2936.

[35] A. Atrian, G. Majzoobi, M. Enayati, H. Bakhtiari, Mechanical and microstructural characterization of Al7075/SiC nanocomposites fabricated by dynamic compaction, Int. J. Miner. Metall. Mater. 21 (3) (2014) 295–303.

[36] P.S. Zangabad, F. Khodabakhshi, A. Simchi, A. Kokabi, Fatigue fracture of frictionstir processed Al–Al3Ti–MgO hybrid nanocomposites, Int. J. Fatigue 87 (2016) 266–278.

[37] S. Raja, M.R. Muhamad, M.F. Jamaludin, F. Yusof, A review on nanomaterials reinforcement in friction stir welding, J. Mater. Res. Technol. 9 (6) (2020) 16459–16487.

[38] S.S. Mirjavadi, M. Alipour, S. Emamian, S. Kord, A. Hamouda, P.G. Koppad, R. Keshavamurthy, Influence of TiO2 nanoparticles incorporation to friction stir welded 5083 aluminum alloy on the microstructure, mechanical properties and wear resistance, J. Alloys Compd. 712 (2017) 795–803.

[39] J. Garay, Current-activated, pressure-assisted densification of materials, Annu. Rev. Mater. Res. 40 (2010) 445–468.

[40] B. Sadeghi, P. Cavaliere, C.I. Pruncu, Architecture dependent strengthening mechanisms in graphene/Al heterogeneous lamellar composites, Mater. Charact. 111913 (2022).

[41] B. Sadeghi, P. Cavaliere, C.I. Pruncu, M. Balog, M. Marques de Castro, R. Chahal, Architectural design of advanced aluminum matrix composites: a review of recent developments, Crit. Rev. Solid State Mater. Sci. (2022) 1–71.

[42] C. Poletti, M. Balog, F. Simancik, H.P. Degischer, High-temperature strength of compacted sub-micrometer aluminium powder, Acta Mater. 58 (10) (2010) 3781–3789.

[43] J. Chen, C. Hao, J. Zhang, Fabrication of 3D-SiC network reinforced aluminum–matrix composites by pressureless infiltration, Mater. Lett. 60 (20) (2006) 2489–2492.

[44] P. Cavaliere, Crack Initiation and Growth in Metal Alloys and Composites, Fatigue and Fracture of Nanostructured Materials, Springer International Publishing, Cham, 2021, pp. 105–154.

[45] N. Han, Z. Wang, L. Sun, Low cycle fatigue behavior of a SiCp reinforced aluminum matrix composite at ambient and elevated temperature, Scr. Metall. Mater. 32 (11) (1995).

[46] S. Mohammed, D. Chen, Z. Liu, Q. Wang, D. Ni, B. Xiao, Z. Ma, Cyclic deformation behavior and fatigue life modeling of CNT-reinforced heterogeneous aluminum based nanocomposite, Mater. Sci. Eng. A 840 (2022), 142881.

[47] B. Sadeghi, M. Shamanian, F. Ashrafizadeh, P. Cavaliere, M. Sanayei, J.A. Szpunar, Microstructural behaviour of spark plasma sintered composites containing bimodal micro- and nano-sized Al2O3 particles, Powder Metall. 61 (1) (2018) 50–63.

[48] B. Sadeghi, M. Shamanian, F. Ashrafizadeh, P. Cavaliere, FSW of bimodal reinforced Al-based composites produced via spark plasma sintering, Int. J. Mater. Res. 108 (12) (2017) 1045–1054.

[49] B. Sadeghi, P. Cavaliere, A. Perrone, Effect of Al2O3, SiO2 and carbon nanotubes on the microstructural and mechanical behavior of spark plasma sintered aluminum based nanocomposites, Part. Sci. Technol. (2018) 1–8.

[50] M. Bodaghi, K. Dehghani, Friction stir welding of AA5052: the effects of SiC nanoparticles addition, Int. J. Adv. Manuf. Technol. 88 (9–12) (2017) 2651–2660.

[51] P. Cavaliere, M. Cabibbo, F. Panella, A. Squillace, 2198 Al–Li plates joined by friction stir welding: mechanical and microstructural behavior, Mater. Des. 30 (9) (2009) 3622–3631.

[52] P. Periyasamy, B. Mohan, V. Balasubramanian, Effect of heat input on mechanical and metallurgical properties of friction stir welded AA6061-10% SiCp MMCs, J. Mater. Eng. Perform. 21 (11) (2012) 2417–2428.

[53] C.J. Hsu, C.Y. Chang, P.W. Kao, N.J. Ho, C.P. Chang, Al–Al3Ti nanocomposites produced in situ by friction stir processing, Acta Mater. 54 (19) (2006) 5241–5249.

[54] U. Anselmi-Tamburini, J. Garay, Z. Munir, A. Tacca, F. Maglia, G. Spinolo, Spark plasma sintering and characterization of bulk nanostructured fully stabilized zirconia: part I. densification studies, J. Mater. Res. 19 (11) (2004) 3255–3262.

[55] U. Anselmi-Tamburini, J. Garay, Z. Munir, A. Tacca, F. Maglia, G. Chiodelli, G. Spinolo, Spark plasma sintering and characterization of bulk nanostructured fully stabilized zirconia: part II. Characterization studies, J. Mater. Res. 19 (11) (2004) 3263–3269.

[56] C. Leon, G. Rodriguez-Ortiz, E. Aguilar-Reyes, Cold compaction of metal–ceramic powders in the preparation of copper base hybrid materials, Mater. Sci. Eng. A 526 (1–2) (2009) 106–112.

[57] F. He, Q. Han, M.J. Jackson, Nanoparticulate reinforced metal matrix nanocomposites – a review, Int. J. Nanopart. 1 (4) (2008) 301.

[58] K. Deng, J. Shi, C. Wang, X. Wang, Y. Wu, K. Nie, K. Wu, Microstructure and strengthening mechanism of bimodal size particle reinforced magnesium matrix composite, Compos. A: Appl. Sci. Manuf. 43 (8) (2012) 1280–1284.

[59] P. Cavaliere, B. Sadeghi, A. Shabani, Spark Plasma Sintering: Process Fundamentals, Spark Plasma Sintering of Materials, Springer, 2019, pp. 3–20.

[60] T. Rajmohan, K. Palanikumar, S. Arumugam, Synthesis and characterization of sintered hybrid aluminium matrix composites reinforced with nanocopper oxide particles and microsilicon carbide particles, Compos. Part B Eng. 59 (2014) 43–49.

[61] K. Dash, D. Chaira, B.C. Ray, Synthesis and characterization of aluminium–alumina micro-and nano-composites by spark plasma sintering, Mater. Res. Bull. 48 (7) (2013) 2535–2542.

[62] S.C. Tjong, Processing and Deformation Characteristics of Metals Reinforced with Ceramic Nanoparticles, 2014, pp. 269–304.

[63] F. Khodabakhshi, A. Simchi, A. Kokabi, A. Gerlich, Similar and dissimilar friction stir welding of an PM aluminum-matrix hybrid nanocomposite and commercial pure aluminum: microstructure and mechanical properties, Mater. Sci. Eng. A 666 (2016) 225–237.

[64] X.G. Chen, M. da Silva, P. Gougeon, L. St-Georges, Microstructure and mechanical properties of friction stir welded AA6063–B4C metal matrix composites, Mater. Sci. Eng. A 518 (1–2) (2009) 174–184.